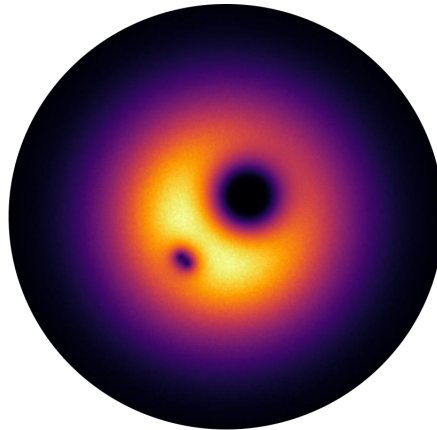




INTERNATIONAL CENTER FOR FUNDAMENTAL PHYSICS, 2ND YEAR OF
MASTER, FINAL INTERNSHIP REPORT

Study of vortices interaction and solitons in a quantum fluid of light



Student:

Simon Lepleux
École Normale Supérieure
simon.lepleux@ens-paris-saclay.fr

Supervisors:

Dr. Quentin Glorieux
Myrann Baker

Quantum Fluids of Light team, Quantum Optics group, Laboratoire
Kastler Brossel, Université Pierre et Marie Curie

June 20, 2024

Contents

1	Introduction	3
2	Quantum fluids of light	4
2.1	Propagation of light in non-linear media	4
2.1.1	From Helmholtz Equation to Nonlinear Schrödinger equation	4
2.1.2	Comoving frame	7
2.2	Mean-field formulation	7
2.2.1	Bogoliubov theory	7
2.2.2	Analogy with the Gross-Pitaevskii equation	9
2.3	Singularities in quantum fluids	10
2.3.1	Vortices	10
2.3.2	Jones-Roberts solitons	11
3	Experimental realization of a quantum fluid of light	12
3.1	Experimental setup	12
3.2	Data processing	13
3.2.1	Amplitude and phase reconstruction	13
3.2.2	Velocity extraction	14
3.3	Results of the "Soliton vs Multivortex" experiment	15
3.3.1	Experimental sequence	15
3.3.2	Measurement of the critical velocity	16
4	Simulation of the evolution of a quantum fluid of light	18
4.1	The nonlinear Schrödinger equation solver	18
4.2	Simulation of the "Soliton vs Multivortex" experiment	18
4.2.1	Time evolution of the field	19
4.2.2	Comparison of the critical velocities	20
5	Conclusion	22

1 Introduction

In the last 30 years, physicists have tried to use the laws of quantum physics to control complex systems, creating what we now call the "second quantum revolution". In this quest for controllable ensembles of quantum systems, platforms like cold gases [?, 1], exciton-polariton condensates [2, 3], superconducting circuits [4], dye-filled cavities [4] or in our case hot atomic vapors [5] were developed.

In this effervescence, quantum fluids of light have emerged as a competitive option due to their relative simplicity and excellent imaging capabilities comparatively to cold gases for instance, where non-destructive measurement of the system is difficult. In fluids of light, the quantum particles are photons whose control is made easy by all the knowledge accumulated during centuries of optics. However, photons do not interact in a vacuum. We thus need to engineer interactions between them using nonlinearities. If these interactions are repulsive, the photons will behave collectively and exhibit fluid-like behavior. Hydrodynamical effects from vortex dynamics [6], dispersive shock waves [7] up to large-scale hydrodynamical phenomena like turbulence [8] were successfully probed in fluids of light.

This internship report contains three sections each dedicated to a different aspect of the study: theory, experiment, and simulation. The first section is devoted to introducing the theoretical concepts and description of paraxial fluids of light. The second section details the experimental observation of singularities in fluids of light and the study of their stability. The third section focuses on a simulation of the dynamics of fluids of light and compares its results with the experiment.

2 Quantum fluids of light

In this section, we will establish the theoretical basis for the concept of fluids of light. Light exhibiting fluid-like behavior was studied during the last 20 years in platforms like micro-cavity exciton polaritons [2], dye-filled cavities [9] or photorefractive crystals [10, 11]. Core features of quantum fluids such as superfluidity [2, 11] or Bose-Einstein condensation [9, 3] were shown to occur in these platforms. In this work, we use a hot atomic vapor cell as a nonlinear medium to generate a quantum fluid of light.

To understand these phenomena, we will first describe the propagation of light in a non-linear medium. We will then look at how we can formulate a mean-field approach to light propagation. Finally, we will describe the different singularities that can appear in a quantum fluid of light. The two first subsections rely heavily on the theoretical framework summarized by Tangui Aladjidi in his recent PhD thesis [12].

2.1 Propagation of light in non-linear media

2.1.1 From Helmholtz Equation to Nonlinear Schrödinger equation

Let us consider the propagation equation of an electric field $\mathbf{E}(\mathbf{r}, t)$ as it passes through a medium. From Maxwell equations, we can derive the starting point of the propagation, the so-called **Helmholtz equation**, whose source term is the electric polarization $\mathbf{P}(\mathbf{r}, t)$ in the medium:

$$\nabla^2 \mathbf{E} - \frac{1}{c^2} \frac{\partial^2 \mathbf{E}}{\partial t^2} = \frac{1}{\epsilon_0 c^2} \frac{\partial^2 \mathbf{P}}{\partial t^2} \quad (1)$$

with c being the speed of light and ϵ_0 the electrical permittivity of vacuum.

The polarization field \mathbf{P} describes the response of the medium to the illumination of the incident field \mathbf{E} . To account for possible nonlinearities, we expand \mathbf{P} in a power series in terms of \mathbf{E} :

$$\mathbf{P}(\mathbf{r}, t) = \epsilon_0 \sum_{n=1}^{\infty} \chi^{(n)} \mathbf{E}^n(\mathbf{r}, t). \quad (2)$$

We define here $\chi^{(n)}$ as the electric susceptibility of the medium. Strictly speaking, $\chi^{(n)}$ is a $n+1$ rank tensor but by taking advantage of various symmetries, one can greatly simplify this expression [13]. Indeed, an atomic vapor is **centrosymmetric** and **isotropic**. This eliminates all even order terms in the expansion of the susceptibility χ . If we limit our expansion to the third order (i.e the first non-linear order), and keep only resonant terms oscillating at ω then the expression in the frequency domain for the electric polarization simply becomes:

$$\mathbf{P}(\mathbf{r}, \omega) = \epsilon_0 \left[\chi^{(1)}(\mathbf{r}, \omega) \mathbf{E}(\mathbf{r}, \omega) + 3\chi^{(3)}(\mathbf{r}, \omega) |E(\mathbf{r}, \omega)|^2 \mathbf{E}(\mathbf{r}, \omega) \right]. \quad (3)$$

We can now rewrite eq.1 in terms of the amplitude E of the field. Assuming a monochromatic light field, we can also simplify this amplitude by separating the envelope and carrier wave $E = \frac{1}{2}(\mathcal{E}e^{i\omega t} + \mathcal{E}^*e^{-i\omega t})$. Looking at the resulting equation for the envelope, we obtain:

$$\nabla^2 \mathcal{E}(\mathbf{r}, \omega) + \frac{\omega^2}{c^2} [1 + \chi^{(1)}(\omega)] \mathcal{E}(\mathbf{r}, \omega) = -\frac{3\omega^2}{4c^2} \chi^{(3)}(\omega) |\mathcal{E}(\mathbf{r}, \omega)|^2 \mathcal{E}(\mathbf{r}, \omega). \quad (4)$$

If we introduce the vacuum wavenumber $k_0 = \omega/c$ of the laser light and the linear index of refraction: $n(\omega) = \sqrt{1 + \chi^{(1)}(\omega)}$. We can thus finally reformulate the previous equation as follows:

$$\nabla^2 \mathcal{E}(\mathbf{r}, \omega) + k(\omega)^2 \mathcal{E}(\mathbf{r}, \omega) + i\alpha k(\omega) \mathcal{E}(\mathbf{r}, \omega) = -\frac{3}{4} \frac{\omega^2}{c^2} \chi^{(3)}(\omega) |\mathcal{E}(\mathbf{r}, \omega)|^2 \mathcal{E}(\mathbf{r}, \omega) \quad (5)$$

where we have defined the medium wavenumber $k(\omega) = k_0 \text{Re}(\sqrt{1 + \chi^{(1)}})$ and the linear absorption coefficient $\alpha = k_0 \text{Im}(\sqrt{1 + \chi^{(1)}})$. We would still like to simplify this equation further to gain more physical insight. For this, we rely on two crucial approximations:

- The **slowly varying envelope approximation**: the envelope \mathcal{E} is a slowly varying function of z relative to the carrier wavelength $\lambda = \frac{2\pi}{k_0}$. This allows to decouple the transverse dynamics of the envelope and the longitudinal dynamics of the carrier such that $\mathcal{E}(\mathbf{r}, z) = \mathcal{E}(\mathbf{r}_\perp, z) e^{ik(\omega)z}$.
- The **paraxial approximation**: the beam will deviate only slightly from the optical axis such that $\partial_z^2 \mathcal{E} \ll k \partial_z \mathcal{E} \simeq \nabla_\perp^2 \mathcal{E}$ meaning that the Laplacian term becomes $\nabla^2 \mathcal{E} \simeq -k^2 \mathcal{E} + 2ik \partial_z \mathcal{E} + \nabla_\perp^2 \mathcal{E}$

These two approximations are at the heart of the physics described in this work and highlight the 2D+1 nature of our geometry (2 space dimensions and 1 time dimension) further detailed in section 2.1.2.

Now in the general case, considering that the laser beam has a certain spectral extension $\delta\omega$, we should consider the effect of dispersion. However, for all of the experiments described in this work, we use a continuous wave (CW) laser, meaning that the spectral extent of our laser light $\delta\omega$ is small compared to ω . The effects of dispersion in the longitudinal axis will then be negligible compared to the evolution in the transverse plane due to interactions. Our system can thus essentially be **considered as 2D+1** through translational invariance of the longitudinal dimension. Switching back to the time domain, we obtain finally the generic propagation equation describing our system:

$$i \frac{\partial \mathcal{E}}{\partial z} = -\frac{1}{2k(\omega)} \nabla_\perp^2 \mathcal{E} - i \frac{\alpha}{2} \mathcal{E} + g(\mathbf{r}_\perp, t) |\mathcal{E}|^2 \mathcal{E}. \quad (6)$$

We can now introduce the non-linear interaction coefficient $g(\mathbf{r}, t) = k_0 \frac{3\chi^{(3)}}{4n(\omega_0)}$ related to the classical **non-linear index of refraction** by $n_2 = \frac{3\chi^{(3)}}{4\epsilon_0 c \text{Re}(n(\omega_0))}$ that has the dimension of m^2/W . We can then derive the non-linear index of refraction variation $\Delta n = n_2 I$ where I is the field intensity. This allows us to link experimental parameters to the interaction strength governing the evolution equation through the measurement of the index of refraction change. If we also include a local variation of the index of refraction $\delta n(\mathbf{r}, z)$, we end up with the final general classical propagation equation, the so-called **non-linear Schrödinger equation** (NLSE):

$$i \frac{\partial \mathcal{E}}{\partial z} = \underbrace{-\frac{1}{2k(\omega)} \nabla_\perp^2 \mathcal{E}}_{\text{Kinetic}} + \underbrace{k(\omega) \frac{\delta n(\mathbf{r}, z)}{n(\omega_0)} \mathcal{E}}_{\text{Potential}} - \underbrace{i \frac{\alpha}{2} \mathcal{E}}_{\text{Losses}} + \underbrace{g(\mathbf{r}, t) |\mathcal{E}|^2 \mathcal{E}}_{\text{Interaction}} \quad (7)$$

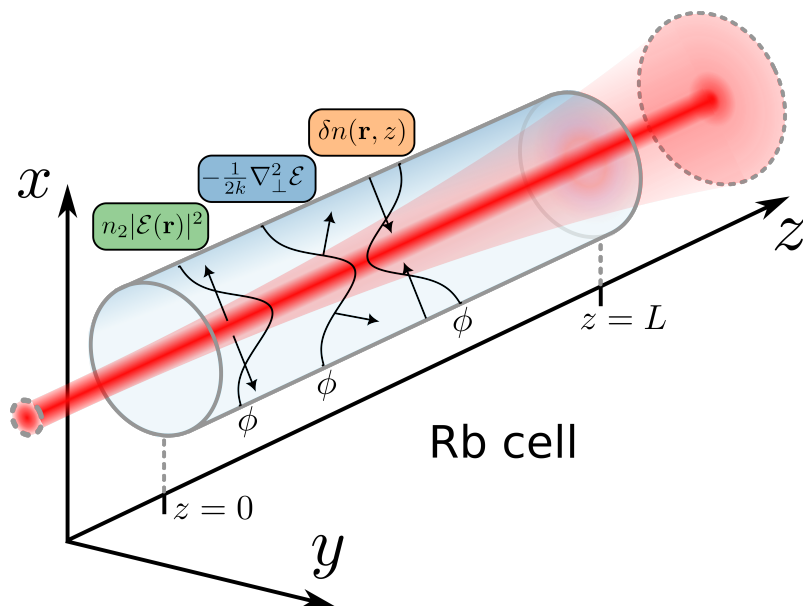


Figure 1: (adapted from [12]) Effect of the different terms of the NLSE. The initial and final transverse profiles are circled by a dotted gray line. The transverse profiles represent the phase resulting from each term, labeled ϕ . Here is represented the case of a negative non-linear coefficient n_2 i.e. a defocusing non-linearity thus expanding the beam. The kinetic energy term in blue highlights the diffraction originating from the double gradient. The potential term in orange depicts the case of a positive δn i.e. an attractive potential.

where we decomposed the equation between all of its constituents: kinetic, potential, and interaction terms. We will now analyze each term of this equation. Looking at eq.7, we identify 4 different terms depicted graphically in fig.1 adapted from [12]:

- **Kinetic energy** (in blue): In the transverse direction, this term corresponds to the curvature of the field and thus describes diffraction.
- **Potential energy** (in orange): A localized index of refraction change acts as a potential for the light field. Assuming a quadratic shape $\delta n \propto r_{\perp}^2$, a negative δn will act as a diverging lens or repulsive potential, while a positive δn will lead to a converging phase profile or attractive potential. In the case of hot atomic vapors, we realize this potential using optical pumping of the D_1 line.
- **Interaction energy** (in green): This is the so-called **Kerr** term describing effects such as self focusing or defocusing. It is often expressed as the non-linear index of refraction variation $\Delta n = g|\mathcal{E}|^2/k_0$ or $\Delta n = n_2 I$. In the case of a positive n_2 non-linear coefficient, with a Gaussian intensity profile $|\mathcal{E}|^2$, this results in a negative phase accumulated (with respect to a reference beam passing through the air) at the high-intensity center of the beam thus focusing it. In the case of a negative n_2 , the opposite effect occurs, and a positive phase is accumulated at the center of the beam resulting in self-defocusing. In this work, we will not study the self-focusing case as it is not energetically stable due to the filamentation effect [14].

- **Losses** (not represented): Linear absorption coefficient due to the imaginary part of the first order susceptibility $\chi^{(1)}$. In this work, this refers to atomic absorption.

We will now reformulate the non-linear equation using a change of referential.

2.1.2 Comoving frame

The situation that we have is the following: we want to study the propagation of a pulse within a dispersive medium. Within the paraxial approximation, the dynamics of the field are confined to transverse planes moving at the group velocity v_g . We are thus tempted to exchange the role of the *actual* time t and the third spatial coordinate z which is an **effective** time. We carry out this variable change by defining the following two new coordinates: an **effective time** $\tau = z/v_g$ and an **effective new dimension** $\zeta = v_g t - z$. By defining a new field ψ depending on the new variables such that:

$$\mathcal{E}(x, y, z, t) = \psi(x, y, v_g \tau, \frac{1}{v_g}(v_g \tau + \zeta)). \quad (8)$$

We thus retrieve a new evolution equation for the field ψ that reads:

$$\frac{i}{v_g} \frac{\partial \psi}{\partial \tau} = -\frac{1}{2k_0} \nabla_{\perp}^2 \psi + V(\mathbf{r}, \tau) \psi + g(\mathbf{r}, \tau) |\psi|^2 \psi \quad (9)$$

where we have substituted the potential term $k(\omega) \frac{\delta n(\mathbf{r}, z)}{n(\omega_0)}$ by $V(\mathbf{r}, \tau)$ for clarity. This is strongly reminiscent of the Gross-Pitaevskii equation (GPE) describing the evolution of interacting bosons [1]. This analogy will be detailed in section 2.2.2.

2.2 Mean-field formulation

Having established the equations for the paraxial propagation of laser light within a non-linear medium, we would like to explain its quantum properties by deriving a quantum version of these equations. For this section, we will rely heavily on seminal works by Pierre-Élie Larré and Iacopo Carusotto who laid the theoretical foundations for the study of quantum fluids of light [15, 16]. The obvious issue in the eq.9, is the nonlinear interaction term that prevents simple integration of this equation. To deal with this, we want to establish first a free field theory that studies the behavior of small amplitude quantum fluctuations on top of a classical mean-field (background). Secondly, we will compare the resulting equation to the GPE for interacting bosons.

2.2.1 Bogoliubov theory

We can look for solutions in the form of:

$$\hat{\mathcal{E}} = \underbrace{\mathcal{E}_0}_{\text{Mean field}} + \underbrace{\delta \hat{\mathcal{E}}}_{\text{Fluctuations}} \quad (10)$$

where the fluctuations operator obeys the usual commutation relations. We know that the evolution of the mean-field is simply described by eq.7. This allows us to retrieve an

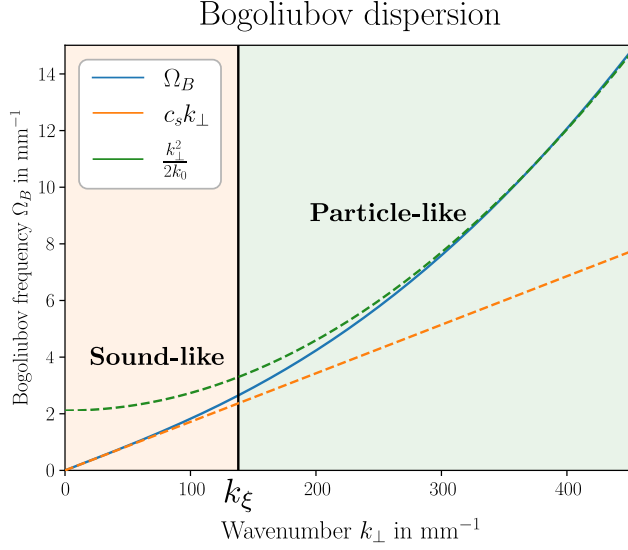


Figure 2: (from [12]) Analytical calculation of the Bogoliubov dispersion Ω_B for typical experimental parameters $n_2 = -5 \times 10^{-9} \text{ m}^2/\text{W}$, $P_0 = 1 \text{ W}$ and $w_0 = 2.35 \text{ mm}$. Only the real part of the dispersion is shown here since the only imaginary part of the function is absorption.

equation for $\delta\hat{\mathcal{E}}$ only. As we want a free field theory, we will truncate to first order. We are thus left with a linearized propagation for the fluctuations [15]:

$$i\frac{\partial\delta\hat{\mathcal{E}}}{\partial z} = -\frac{1}{2k_0}\nabla_{\perp}^2\delta\hat{\mathcal{E}} + g(\mathbf{r}, z) \left[2|\mathcal{E}_0|^2\delta\hat{\mathcal{E}} + \mathcal{E}_0^2\delta\hat{\mathcal{E}}^{\dagger} \right] - i\alpha\delta\hat{\mathcal{E}}. \quad (11)$$

As it is, direct integration of this equation is impractical. Indeed, we can rewrite it in the form of a matrix acting on the vector $(\delta\hat{\mathcal{E}}, \delta\hat{\mathcal{E}}^{\dagger})$, but this matrix is not diagonal. We thus use the **Bogoliubov transform** [1] to introduce new operators $\hat{b}_{\mathbf{k}_{\perp}}$ called the Bogoliubov quasi-particles. The $\hat{b}_{\mathbf{k}_{\perp}}$ operators are the eigenmodes of the evolution matrix and their eigenvalue is the Bogoliubov dispersion [17]. The spectrum of the transformation yields:

$$\Omega_B(\mathbf{k}_{\perp}) = \sqrt{\frac{\mathbf{k}_{\perp}^2}{2k_0} \left(\frac{\mathbf{k}_{\perp}^2}{2k_0} + 2g|\mathcal{E}_0|^2 \right)} - i\frac{\alpha}{2}. \quad (12)$$

This dispersion relation is represented in fig.2 and has several major features crucial for understanding the dynamics of quantum fluids. It is divided into two regions separated by the typical scale $k_{\xi} = \sqrt{k_0 g |\mathcal{E}_0|^2} = k_0 \sqrt{\Delta n} = \frac{2\pi}{\xi}$ where ξ is the **healing length**:

- A **linear** sonic region under k_{ξ} where $\Omega_B(\mathbf{k}_{\perp}) \approx c_s k_{\perp}$ with $c_s = c\sqrt{g|\mathcal{E}_0|^2/k_0} = c\sqrt{\Delta n}$ defining the speed of sound.
- A **quadratic** particle-like region above k_{ξ} where $\Omega_B(\mathbf{k}_{\perp}) \approx \frac{\mathbf{k}_{\perp}^2}{2k_0}$.

The healing length ξ represents the scale under which we can no longer consider the fluid as a collective ensemble. The corresponding momentum scale k_ξ represents the critical momentum at which superfluidity breaks down. It also has profound meaning in atomic Bose-Einstein condensates, where excitations under the healing length kick atoms out of the condensate [1].

The existence of sound-like excitations in fluids of light has dramatic implications that cannot be described well within the language of non-linear optics. Such a striking phenomenon has been observed experimentally by Quentin Fontaine in [17]. We have thus seen in this section that the photon-photon interactions that are mediated by the atom-light interaction within the vapor introduce effects that go beyond classical non-linear optics treatments, and rather fall in the phenomenology of cold atomic ensembles. With this in mind, I will now detail this comparison with cold Bose gases to extract meaningful insight from what has been a very successful experimental platform for quantum physics these last twenty years.

2.2.2 Analogy with the Gross-Pitaevskii equation

It is known bosonic atoms condense below a certain critical temperature into a Bose-Einstein condensate (BEC). Experimentally, this phenomenon is realized by cooling down atoms in optical traps using a wide range of techniques pioneered by Claude Cohen-Tannoudji, Steven Chu, and William Daniel Phillips granting them the 1997 Nobel Prize. Since the first experimental observation of a BEC in 1995 at JILA [18], many groups have carried out similar research to study effects such as superfluidity and supersolidity. One can show [1] that the equation governing the wavefunction of atoms in a BEC is the **Gross-Pitaevskii equation** (GPE):

$$i\hbar \frac{\partial \Psi}{\partial t} = \frac{\hbar^2}{2m} \nabla^2 \Psi + V\Psi + g|\Psi|^2\Psi \quad (13)$$

where m is the atomic mass, V is the confining potential, g the interaction constant. We can then use the Bogoliubov formalism as in section 2.2.1 to recover the Bogoliubov dispersion where the energy of the Bogoliubov excitations at momentum p is:

$$\hbar\omega(p) = \sqrt{\frac{p^2}{2m} \left(\frac{p^2}{2m} + 2g\rho_0 \right)} \quad (14)$$

assuming that ρ_0 is the condensate density. From the dispersion relation, we can derive the **healing length** $\xi = \hbar/\sqrt{2mg\rho_0}$ and the speed of sound $c_s = \sqrt{g\rho_0/m}$. We now have common units of space and speed to compare the evolution of fluids of light and cold atomic ensembles.

At this stage, we recall that in section 2.1.2 we introduced a basis change substituting time and z dimensions and recovered the full 2D+1 evolution equation of the fluid of light described by eq.9. We notice that the NLSE in the comoving frame is **mathematically equivalent** to the GPE in 2 dimensions.

We can now already identify the equivalent terms in both GPE and NLSE. In the case of BEC, the interaction parameter is the chemical potential $\mu = g\rho_0$. From the comparison of eqs.9 and 13 we find that the equivalent parameter for fluids of light is $\hbar cg|E_0|^2 = \hbar\omega_0\Delta n$. To give numerical orders of magnitude, trapping frequencies in typical BEC experiments

are in the kHz range [19]. In our case, typical values of the non-linear dephasing are $\Delta n \sim 10^{-5}$, corresponding to a frequency in the 10 GHz range. This means that typical interactions in a photon fluid are **seven orders of magnitudes larger** than in atomic BECs. This explains why it is possible to observe much of the same physics as Bose gases even though the interaction times are much smaller (travel time through the Rubidium cell is on the order of a few 100 ps compared to the millisecond to second time scale used in cold atoms experiments).

2.3 Singularities in quantum fluids

The NLSE is at the heart of several hydrodynamics effects like rogue waves, solitons[20, 2] and vortices [21]. It is then natural to recast the previous equation 7 to a hydrodynamics formulation. We rewrite the complex field of the electric field envelope \mathcal{E} as follows [22]:

$$\mathcal{E}(\mathbf{r}_\perp, z) = \sqrt{\rho(\mathbf{r}_\perp, z)} e^{i\Phi(\mathbf{r}_\perp, z)}. \quad (15)$$

We can now define the velocity of the field as $\mathbf{v} = \frac{c}{k_0} \nabla \Phi(\mathbf{r}_\perp, z)$. In this way, speed is essentially the instantaneous wavevector of the field i.e. the direction in which it will evolve. Plugging this relation into eq.7, we retrieve the well known quantum **Euler equations** [22]:

$$\frac{\partial \rho}{\partial z} = -\frac{1}{c} \nabla_\perp (\rho \mathbf{v}) - \alpha \rho \quad (16)$$

$$\frac{\partial \mathbf{v}}{\partial z} = -\frac{1}{2c} \nabla_\perp \mathbf{v}^2 - \frac{c}{k_0} \nabla_\perp \left(g\rho - \underbrace{\frac{1}{2k_0} \frac{\nabla_\perp^2 \sqrt{\rho}}{\sqrt{\rho}}}_{\text{Quantum pressure}} + V \right) \quad (17)$$

Now that we have a hydrodynamical formulation for the evolution of the field \mathcal{E} , we will describe the singularities that can exist inside this quantum fluid.

2.3.1 Vortices

Quantum vortices are local topological defects exhibited in superfluids and superconductors. In superfluids, a quantum vortex "carries" quantized orbital angular momentum ℓ . We know from [23] the wavefunction for a vortex of charge ℓ centered at the origin in polar coordinates:

$$\Psi_\ell(r, \theta) = \sqrt{\rho_0} \left(\frac{r}{\sqrt{r^2 + \xi^2/\Lambda^2}} \right)^{|\ell|} e^{i\theta\ell} \quad (18)$$

$$\mathbf{v}_\ell(r, \theta) = \frac{c}{k_0} \nabla \Phi = \frac{c}{k_0} \frac{\ell}{r} \mathbf{u}_\theta \quad (19)$$

where ρ_0 is the background fluid density, ξ the healing length and Λ is a constant $\simeq 0.82$. The density and phase of the quantum fluid around a vortex of charge $\ell = 1$ are represented in fig.3(a) and (b). We observe that the phase winds around a density hole at the center of the vortex reminding the characteristics of optical vortices [24]. We plot the velocity field \mathbf{v} generated by the vortex in fig.3(c) on top of which we show a colormap of $|\mathbf{v}|$. We obtain an irrotational flow as expected from 19 where velocity is orthoradial and peaks

at the center of the vortex. Vortices of charge $\ell > 1$ can be generated in quantum fluids but are shown to be unstable [25]. After a critical time, they will break into lower-charge vortices until only a collection of $\ell = 1$ vortices remains.

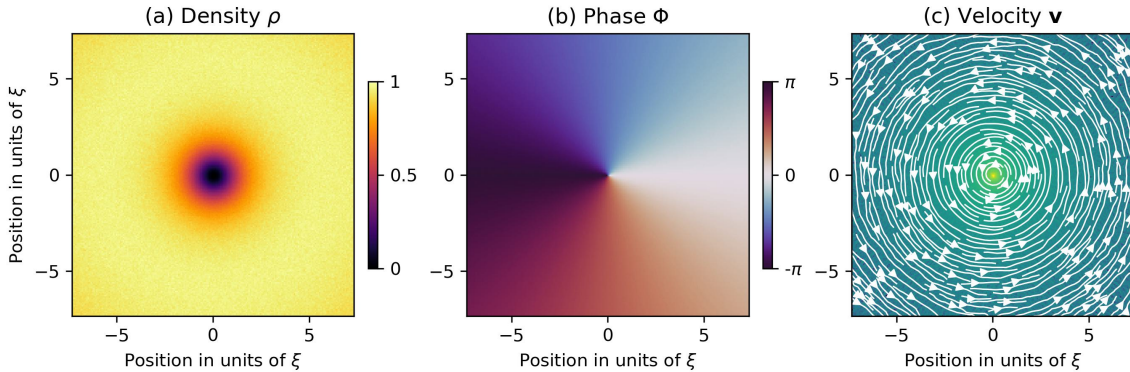


Figure 3: Numerical simulation of the wavefunction of a quantum vortex of charge $\ell = 1$: (a) density of the wavefunction, (b) phase of the wavefunction, (c) white arrows: velocity field generated by the phase gradient, background: norm of the velocity (log scale)

2.3.2 Jones-Roberts solitons

A soliton is a localized wavepacket that propagates in a field without deformation. It can exist in material fields [26], BECs [27], optical fields [28] or even magnets [29]. We call a soliton "bright" (resp. "dark") when it generates a peak (resp. a gap) of intensity at its center. In 1D, solitons are stable solutions of the propagation equation. In 2D however, solitons tend to deform and break apart due to what is commonly called the "snaking" instability [30].

A few decades ago, a special class of dark quasi-solitons was theorized: Jones-Roberts solitons (JRS) [31]. They are the only known class of stable dark solitonic solutions of

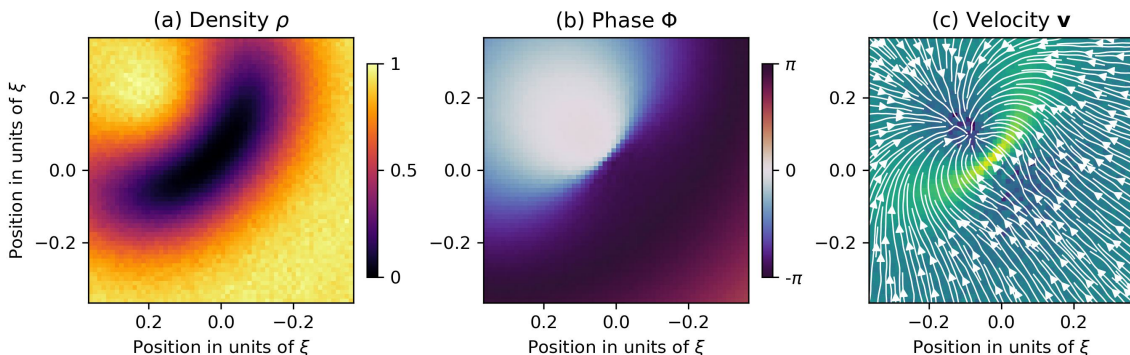


Figure 4: Numerical simulation of the wavefunction of a Jones-Roberts soliton: (a) density of the wavefunction, (b) phase of the wavefunction, (c) white arrows: velocity field generated by the phase gradient, background: norm of the velocity (log scale)

the NLSE in two and three dimensions. They feature a distinctive elongated elliptical shape that allows them to travel without change of form. Observations of JRSs have been reported in BECs but remain elusive [32]. Recently, our group has been able to generate stable structures in fluids of light resembling a JRS via merging two vortices of opposite charge ℓ (equivalently called a dipole). The wavefunction of this singularity is represented in fig 4(a) and (b). We observe the characteristic elliptical shape for the density of the JRS and notice that the phase doesn't present any discontinuities, contrary to vortices. The (c) panel of fig.4 shows that the norm of the fluid velocity increases around the center of the JRS. If we study the merging of a vortex dipole, we notice that the direction of the flow in the center of the dipole reverses when the two vortices merge to become a soliton. This property will be of particular interest in section 3.3.2.

Fig.3 and 4 were obtained via a numerical solver of NLSE described in more detail in section 4.1. We will now explain how to generate and study the dynamics of these singularities in the context of paraxial fluids of light.

3 Experimental realization of a quantum fluid of light

A wide variety of platforms allow us to study the dynamics of fluids of light. One can think of micro-cavity exciton polaritons [2], dye-filled cavities [9] or photorefractive crystals [10, 11]. Some of the most striking features of quantum fluids such as superfluidity [2, 11] or Bose-Einstein condensation [9, 3] have already been observed experimentally on these platforms. In this work, we chose to work with a hot atomic vapor cell as nonlinear media because it yields several advantages compared to photorefractive crystals or exciton-polaritons. Indeed, the above-mentioned platforms show much lower tunability in the nonlinearity and their properties are highly sample dependent. Additionally, hot atomic vapor cells do not require vacuum chambers and cryostats thus allowing a simpler implementation.

We will start this section by describing the experimental setup used in our group to observe the dynamics of the quantum fluid of light. We will then explain how we process the data to extract meaningful hydrodynamic observables. We will finish by showcasing the results of an original experiment realized during my internship on the interaction of multivortices and Jones-Roberts solitons.

3.1 Experimental setup

Experimental observation of quantum fluids of light is made possible by using an interferometer in a Mach-Zehnder configuration represented in fig.5 taken from [12]. Laser light generated by a 2W 780nm laser is first split in two different optical paths thanks to a polarizing beamsplitter (PBS):

- A high power **fluid beam** is transmitted by the PBS and reflected on a spatial light modulator (SLM). The SLM is controlled by a computer, it manipulates both the amplitude and the phase of the reflected beam allowing the impression of specific wavefunctions into the beam profile. The fluid beam then goes through a 4f system serving two purposes. We use it firstly to image the plane of the SLM onto the input face of the rubidium cell. Secondly, a pinhole located at the focal point of the 4f

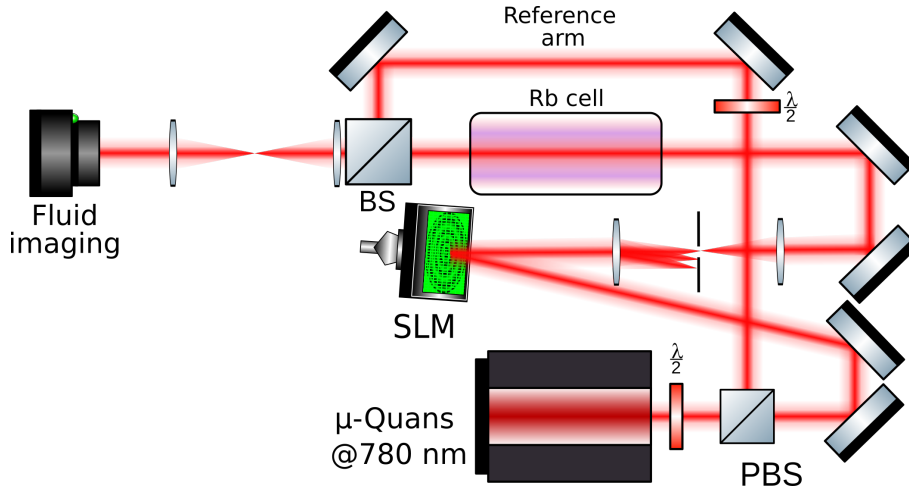


Figure 5: Experimental setup for quantum fluid of light generation in hot atomic vapor

system filters all undesired orders of diffraction resulting from the reflection on the SLM. The fluid beam then penetrates a 20 cm long Rb cell stabilized at 150°C where the nonlinear effects take place. At this temperature, the density of atoms inside the cell approaches 10^{14} atoms/cm³. The fluid beam is then recombined with the other beam thanks to another PBS.

- A low power **reference beam** is guided directly to the recombination PBS and will act as a phase reference.

After recombination, the output plane of the Rb cell is imaged on a CCD camera by a 4f system. The reference beam is overlapped with the fluid beam at an angle allowing to separate the interference pattern numerically. This is the so-called "off-axis" interferometry technique detailed further in section 3.2.1. The recovery of interference is also made easier by the large diameter of the reference beam acquired during its propagation.

3.2 Data processing

The final image collected by the CCD camera does not allow itself to observe the fluid of light. A further step of data processing is necessary to extract meaningful information such as density ρ , phase Φ , and velocity \mathbf{v} of the fluid.

3.2.1 Amplitude and phase reconstruction

The intensity pattern on the camera resulting from the overlap of the fluid and reference beams can be written as follows:

$$I_{\text{tot}} = I_{\text{fluid}} + I_{\text{ref}} + 2\sqrt{I_{\text{fluid}}I_{\text{ref}}}\cos(\mathbf{k}_r\mathbf{r}_\perp + \phi(\mathbf{r}_\perp)) \quad (20)$$

where I_{fluid} and I_{ref} are respectively the intensities of the fluid and the reference beam, \mathbf{k}_r is the wavevector of the reference beam and $\phi(\mathbf{r}_\perp)$ is the phase accumulated by the fluid beam at position \mathbf{r}_\perp . The presence of an angle between the fluid and the reference beam

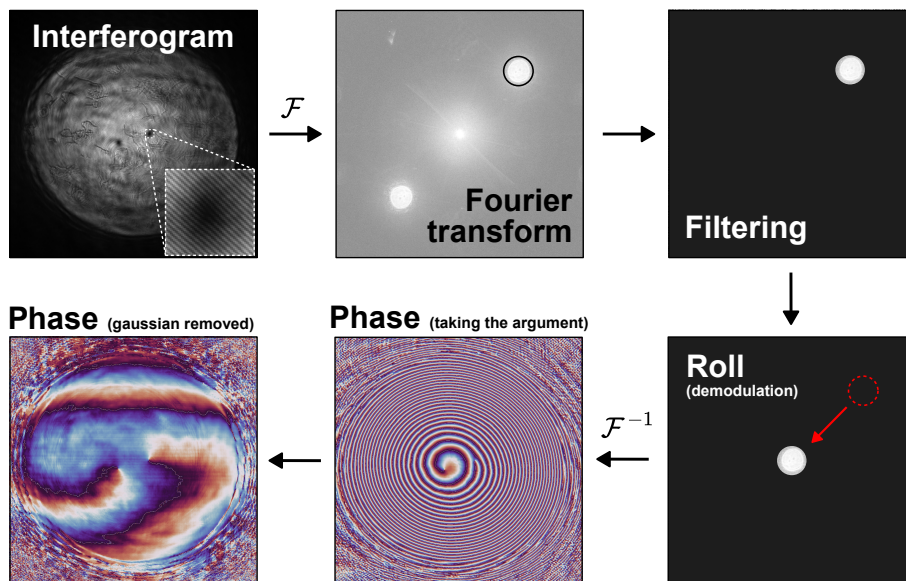


Figure 6: Procedure to extract the phase of the beam out of the Rb cell. We first perform a Fourier transform of the camera image, then filter out the low-frequency part. Inverse Fourier transform allows us to retrieve the phase. The Gaussian background can then be removed to observe the singularities.

allows to extract the meaningful information $\phi(\mathbf{r}_\perp)$ from the offset by **demodulating** the signal centered at the frequency \mathbf{k}_r . An example of the demodulation process is represented in fig.6 for the case of a flow containing two vortices. We first Fourier transform the image and apply a circular mask onto the peak at frequency \mathbf{k}_r . The resulting image is then translated and we perform an inverse Fourier transform. The resulting field is now **free from any offset component** and contains all the information on the density ρ and phase Φ of the quantum fluid, as described in eq.15.

Due to the Gaussian intensity profile of the beam, the phase accumulated due to the nonlinearity $n_2 I$ at the center of the beam is different from the one at the edges. To observe the dynamics of singularities in the flow, it can be useful to remove that background phase shift. To do so, we measure this shift from a Gaussian beam with no singularities and subtract it from the previously extracted phase. This process results in a phase image containing only signatures of the singularities and is represented in the last panel of fig.6.

3.2.2 Velocity extraction

We know from section 2.3 that we can define a **fluid velocity** as $\mathbf{v} = \frac{c}{k_0} \nabla \Phi$. However, applying this definition to the measured phase would generate divergences since the phase is periodic and suddenly jumps from 0 to 2π at many points of the fluid. To tackle this issue, we perform a so-called "unwrapping" of the phase that destroys these discontinuities. Concretely, the unwrapping is done thanks to built-in Python libraries that shift the phase by 2π when a jump is detected. After unwrapping we get a perfectly smooth phase pattern and we use the definition of \mathbf{v} to obtain the velocity field.

The values obtained for velocity are not meaningful by themselves. If we want to compare

our system to other quantum fluids we would like to use **adimensional quantities**. The most straightforward way to adimensionalize velocity is to compare it to the speed of sound in the medium c_s defined in section 2.2.1 as $c_s = c\sqrt{\Delta n}$. From now on, all the velocities presented in the following sections will be given in units of c_s .

3.3 Results of the "Soliton vs Multivortex" experiment

Fluids of light offer advantageous resolution and control compared to conventional cold atoms experiments. These benefits allow us to study more in-depth the dynamics of quantum fluids and their singularities. It is for instance possible to observe interactions at a distance and collisions of objects such as solitons and vortices [12, 28]. In the bloodline of these experiments, I tried to study the evolution of a Jones-Roberts soliton interacting with a large multivortex (ℓ up to 15). This experiment was motivated by the observation of a **JRS breaking into a vortex pair of opposite charges** (probably due to the fast flow generated by the MV) and was baptized the "Soliton versus MultiVortex" (SMV) experiment. It aims at understanding the mechanisms ruling JRS breaking and measuring precisely the velocities at which this effect occurs. These results could then be compared to the theoretical values obtained by Smirnov and Mironov in [33].

3.3.1 Experimental sequence

The SMV experiment was constituted by a sequence of 3 steps where we observed for each step the field at the output of the cell:

- A first step where we input a **JRS and a MV** of increasing charge ℓ at the entrance of the cell with the SLM. At the end of this step, 15 images are taken with $\ell \in \llbracket 1, 15 \rrbracket$.

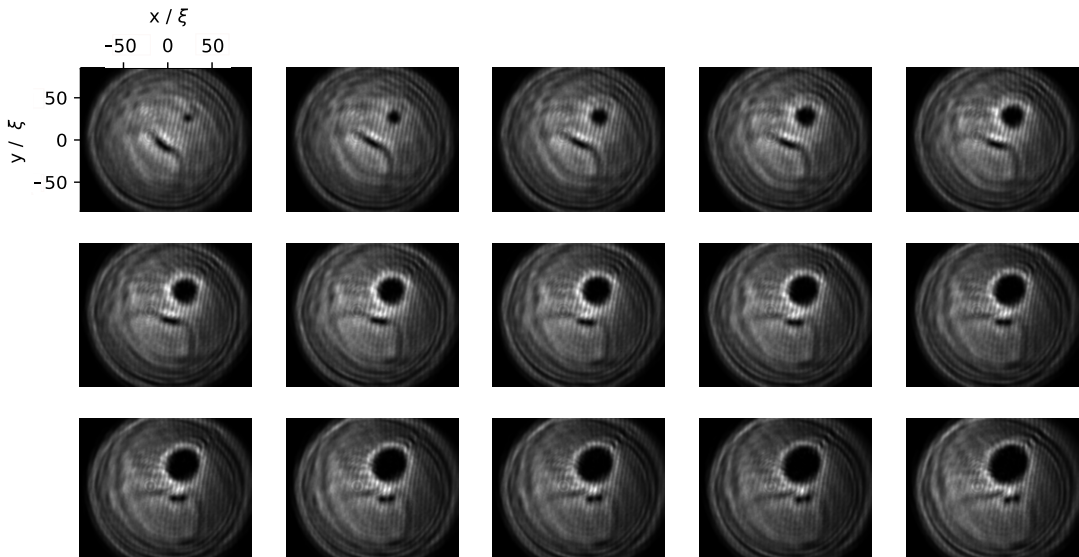


Figure 7: Mosaic representing in the reading direction the evolution of the density of the fluid in the SMV experiment. Each panel corresponds to a MV charge $\ell \in \llbracket 11, 15 \rrbracket$

- A second step where **only the MV** is generated by the SLM allowing to observe the background flow that it produces for each ℓ .
- A third and last step where **no singularities** are produced. We thus observe the Gaussian background of the beam allowing for phase extraction (see section 3.2.1).

Density from the first step is displayed in figure 7. In the first row, the multivortex is small ($\ell \in \llbracket 1, 5 \rrbracket$) and we observe the JRS moving to the right due to the anticlockwise rotating flow. On the second row, we notice that the JRS splits into two vortices while still being dragged to the right by the current. The two vortices then keep moving and separate even more on the third row where $\ell \in \llbracket 11, 15 \rrbracket$. We notice here that density measurements give only a hint of the physics at play in this experiment. We will now study thoroughly the dynamics of the JRS breaking mechanism by extracting the phase and velocity of the fluid.

3.3.2 Measurement of the critical velocity

Data from the first step of the SMV experiment allows us to obtain the JRS velocity \mathbf{v}_{jrs} using the extraction method explained in section 3.2.2. To do this, we average the measured velocity on a 10 px wide square window located on the JRS. We perform the same measurement on data from the second step of the experiment to extract the background velocity \mathbf{v}_{bg} at the position of the JRS. It is now straightforward to calculate the relative velocity \mathbf{v}_{r} of the JRS with respect to the background flow as:

$$\mathbf{v}_{\text{r}} = \mathbf{v}_{\text{jrs}} - \mathbf{v}_{\text{bg}}. \quad (21)$$

The results of this analysis are summarized in fig.8. In panel (a) are represented the velocities of the JRS and the background for increasing MV charge. We observe that $|\mathbf{v}_{\text{bg}}|$ grows linearly with ℓ as theoretically described in eq.19. In a different way, $|\mathbf{v}_{\text{jrs}}|$ increases for ℓ below $\ell = 6$ and then decreases. This behavior can be explained if we observe the x and y components of \mathbf{v}_{r} represented fig.8(b). We observe a **massive jump** from $0.6 c_s$ to $-0.8 c_s$ in the value of \mathbf{v}_{r}^y when $\ell = 6$. A smaller jump also occurs for \mathbf{v}_{r}^x . We know from section 2.3.2 that this corresponds to the reversal of the central velocity of the dipole when the transition from a JRS to a vortex pair occurs.

Knowing that the JRS splits for a MV of charge $\ell = 6$ we can explain the decrease in velocity observed in panel (a): as the vortex pair dissociates due to the background flow, the distance between the vortices is rising and therefore they slow down [33]. In panel (c) we finally plot the relative velocity \mathbf{v}_{r} with respect to the background velocity \mathbf{v}_{bg} to extract the velocity for which the breaking occurs: approximately **0.8 c_s** . This result is not to be taken as a general answer to the JRS breaking puzzle. Indeed, numerous factors need to be taken into account before trumpeting the results of the experiment:

- First of all, we observed that the result is **sensitive to the computational window size** up to 10 %. This parameter is nonphysical and a clear definition of the optimal window size to measure the velocity of a JRS should be given. Smirnov & Mironov give a possible answer to this question in [33] when they define a velocity parameter \bar{v} computed via an integration of the total wavefunction.

3.3 Results of the "Soliton vs Multivortex" experiment

- Secondly, none of the flows present in the SMV experiment are trivial. The irrotational flow generated by the MV and the JRS flow are not propagating in the same direction implying an angle between them. This is **not the simplest way** to study the dynamics of JRS breaking and could influence the result. One could try to make the JRS evolve in a simple uniform flow and extract the velocity at which breaking occurs. These experiments were not performed during my internship because of the lack of time.
- Lastly, it is known that solitons are sensitive to **variations in the fluid density** ρ [33]. Yet, the inhomogeneity of the background density due to the Gaussian shape of the beam is not taken into account in the SMV experiment.

Despite these flaws in the SMV experiment, it still is one of the first experimental observations of a Jones-Roberts soliton in a quantum fluid and the first time we can test their stability through breaking dynamics. These advances are made possible by the unique resolution and experimental control available in the study of fluids of light.

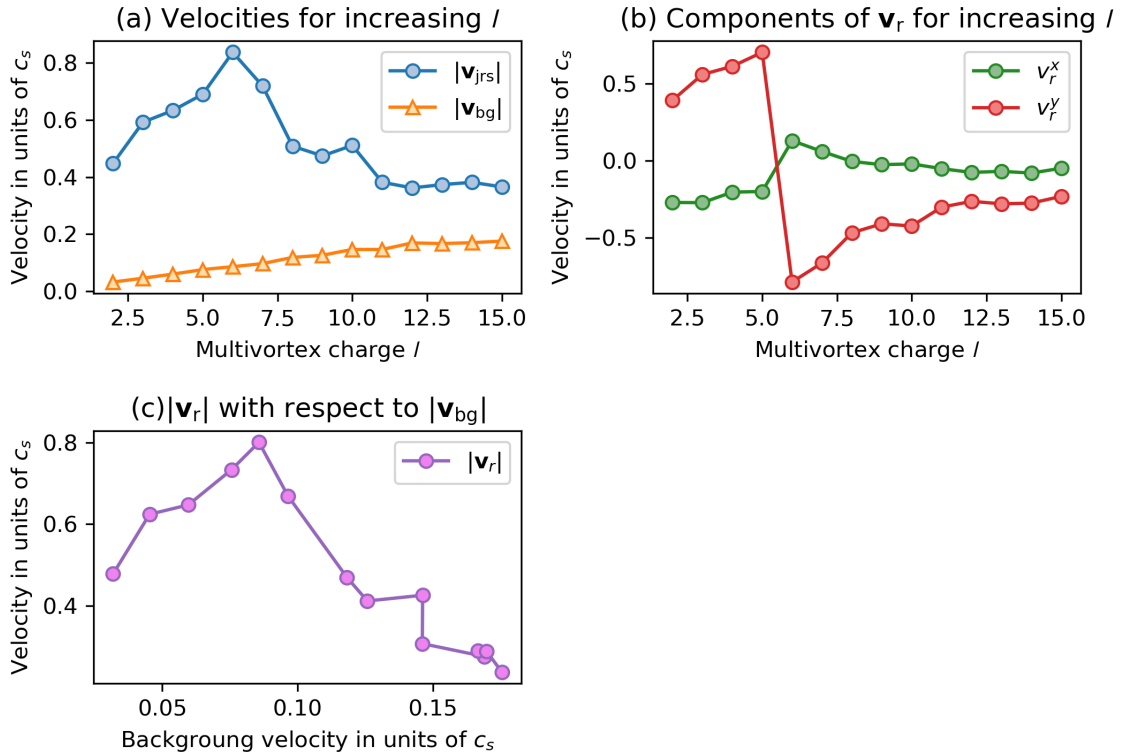


Figure 8: Results of the SMV experiment. (a) Evolution of the JRS and background velocities for increasing MV charge, (b) evolution of the components of \mathbf{v}_r for increasing MV charge, (c) norm of \mathbf{v}_r with respect to the background velocity

4 Simulation of the evolution of a quantum fluid of light

To get a better physical insight into the dynamics of soliton breaking, it is useful to try and simulate the evolution of the field in **effective time** τ . Indeed, the results of the SMV experiments give the relative velocity at which JRS breaking occurs, but they do not allow us to *actually observe* the breaking in real-time. To this mean, we will use a numerical solver of the NLSE developed in the group by Tangui Aladjidi (available at [quantum-optics-lkb.github.io/NLSE/](https://github.com/quantum-optics-lkb/NLSE/)) to reproduce the results of the SMV experiment. In this section, I will first describe the working principles of the numerical solver for NLSE. I will then compute the evolution of the field and the critical velocities in a numerical analog of the SMV experiment.

4.1 The nonlinear Schrödinger equation solver

To solve the NLSE, we use a spectral split-step method [34]. We first reformulate the general NSLE (eq.7) into an "Euler" or "Runge-Kutta" type of equation:

$$\frac{d\psi}{dz} = \left(i\frac{1}{2k_0}\nabla^2 - iV - ig|\psi|^2 \right) dz. \quad (22)$$

This form allows the integration of the equation over a small step δz to obtain:

$$\psi(z + \delta z) = e^{\left(i\frac{1}{2k_0}\nabla^2 - iV - ig|\psi|^2 \right)\delta z} \psi(z). \quad (23)$$

We can thus compute the field after a small propagation step using a simple matrix multiplication. However, we have to keep in mind that the exponential contains matrices and cannot simply be split into a product. To tackle this issue, we use the Baker-Hausdorff formula and keep only first-order terms in δz . We end up with a product of two exponentials $e^L e^N$ where L is the laplacian part $i\frac{1}{2k_0}\nabla^2$ and N the nonlinear part $-iV - ig|\psi|^2$, this is the **split-step** method.

We perform one last trick by applying the Laplacian part in Fourier space where $\nabla = i\mathbf{k}$. We transform back the obtained matrix in the real space and multiply it by the nonlinear term, this is the **spectral method** [35]. This scheme results in accuracy up to $O(\delta z)$. Nonetheless, errors can be reduced up to $O(\delta z^3)$ using the "leap-frogging" method where half of the nonlinear step is applied before the linear part, and half after [36].

4.2 Simulation of the "Soliton vs Multivortex" experiment

Before performing a numerical simulation of the SMV experiment I had to extract the relevant experimental parameter used during the experiment: the nonlinear index of refraction n_2 , the beam waist w and power p , and finally the saturation intensity I_{sat} at which the laser field saturates Rb atoms. These parameters are easily obtained by measuring the evolution of the refractive index variation Δn with respect to P .

After plugging the measured values in the simulation, I only needed to reproduce the input field generated by the SLM containing a multivortex and a Jones-Roberts soliton at the right position and with the right charge ℓ . The simulated field evolved very similarly to the experimental data proving that the experimental parameters were **measured accurately**. A comparison between the simulation results and the experiment is represented

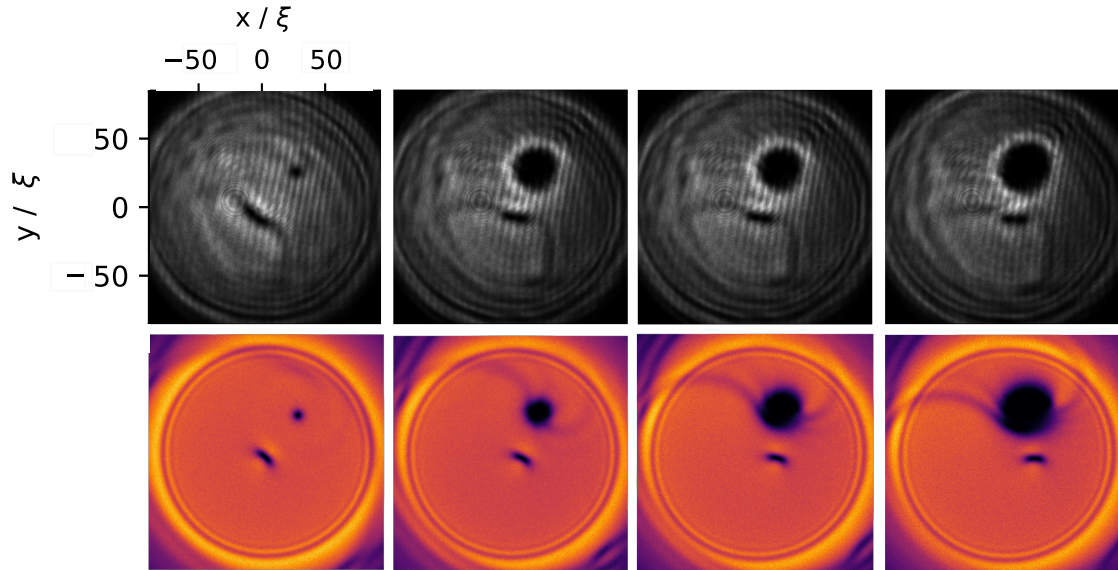


Figure 9: Mosaic representing in the reading direction the evolution of the density of the fluid in the SMV experiment (first row) and in the simulation (second row). Each panel corresponds to a MV charge $\ell \in [1, 4, 7, 10]$.

in fig.9. We see that the final position of the JRS and the MV in the field are relatively similar, we can explain the small inconsistencies by the imprecision in the measurement of the experimental parameters. On top of the distinctive singularities, we notice the presence of **additional wavelets** whose origin will be explained in the next subsection. One crucial feature of the simulation is the observation of the JRS breaking into a vortex pair when the charge of the MV is $\ell = 7$. Breaking is clearly observed in the phase of the simulated field (not shown here). In the $\ell = 6$ simulation, the phase does not present any discontinuities while for $\ell = 7$ we observe a 2π winding of the phase at two different locations. This value of $\ell = 7$ is close to the experimental value of $\ell = 6$. However, we need to push the comparison further by calculating the observable of interest: the **relative velocity** \mathbf{v}_r at which breaking occurs. We will execute this task in section 4.2.2.

4.2.1 Time evolution of the field

The advantage of a simulation is that it allows to monitor the evolution of the fluid as it propagates inside the cell. This is particularly useful for us as we would like to observe the very instant where the JRS breaks into a dipole. Indeed, if strong hints lead us toward the hypothesis of a JRS breaking into a vortex pair during the evolution in the nonlinear medium, **it has not been observed** in the experiment where we only obtained the field at the output of the cell.

To this end, we extract the field at different effective times τ (or equivalently different positions z) in a simulated run where the JRS appears broken after propagation. In fig.10 we plot the density and phase of the field at two different positions z for a run where the charge of the MV is $\ell = 10$. For better visibility in this figure, discontinuities of the phase are represented by sharp white lines. Panel (a) shows a zoom on the JRS density

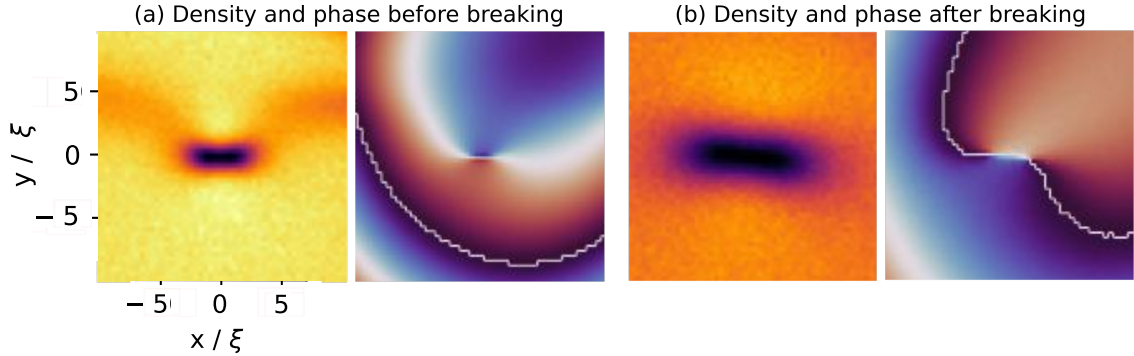


Figure 10: Simulation of a Jones-Roberts soliton breaking into a vortex pair. (a) Zoom on the density and phase of the fluid after $z = 7$ cm inside the cell. The phase shows no discontinuity. (b) Density and phase of the fluid after $z = 13$ cm inside the cell. We observe two discontinuities in the phase. All images have the same spatial scale.

and phase at $z = 7$ cm. We notice that the phase does not present any discontinuity at the location of the JRS. On the other side in panel (b) we observe a discontinuity line going through the JRS and a 2π winding of the phase at two different locations. This panel represents the field at $z = 14$ cm proving that **breaking indeed occurs** during the propagation. If we study the intermediate steps between these two positions, we witness the two singularities appearing extremely close to each other and slowly separating with time.

Another dynamic that we observe in the simulation is the generation of ripple-like waves at the surface of the fluid around singularities. These waves appear at the very start of the run and are damped while they propagate. We can see those ripples in fig.9 where they seem to be deflected by the massive multivortex and dragged along by its flow. My interpretation is that these ripples are resulting from **the quench of interaction** at the entrance of the cell, an effect that has been studied thoroughly in [12]. Indeed, as the fluid enters the cell it encounters the nonlinear medium straight away without time for an adiabatic evolution. Structures in the fluid such as vortices thus have to adapt to the new Hamiltonian and emit sound waves as a consequence. These sound waves can even be seen in the experimental data in fig.7 and 9 but less distinctly due to noise.

4.2.2 Comparison of the critical velocities

At this point in my work, I have all the tools to compare the results of the SMV experiment with a tailored simulation. To this mean, I simulate the first two steps of the SMV experiment as detailed in section 3.3.1. One simulation is done with a JRS and a MV of charge $\ell = 10$, and another with only the MV. In reality, due to the detection algorithm used to locate the JRS in the field and the limited precision of the split-step method, the simulated data appears a bit noisy. To counteract this effect we perform multiple simulations with the same initial conditions and **average them out** to obtain smoother data.

To measure adimensional velocities, we extract from the simulated runs without JRS the speed of sound c_s as the field evolves in τ (or equivalently z). The results are given in

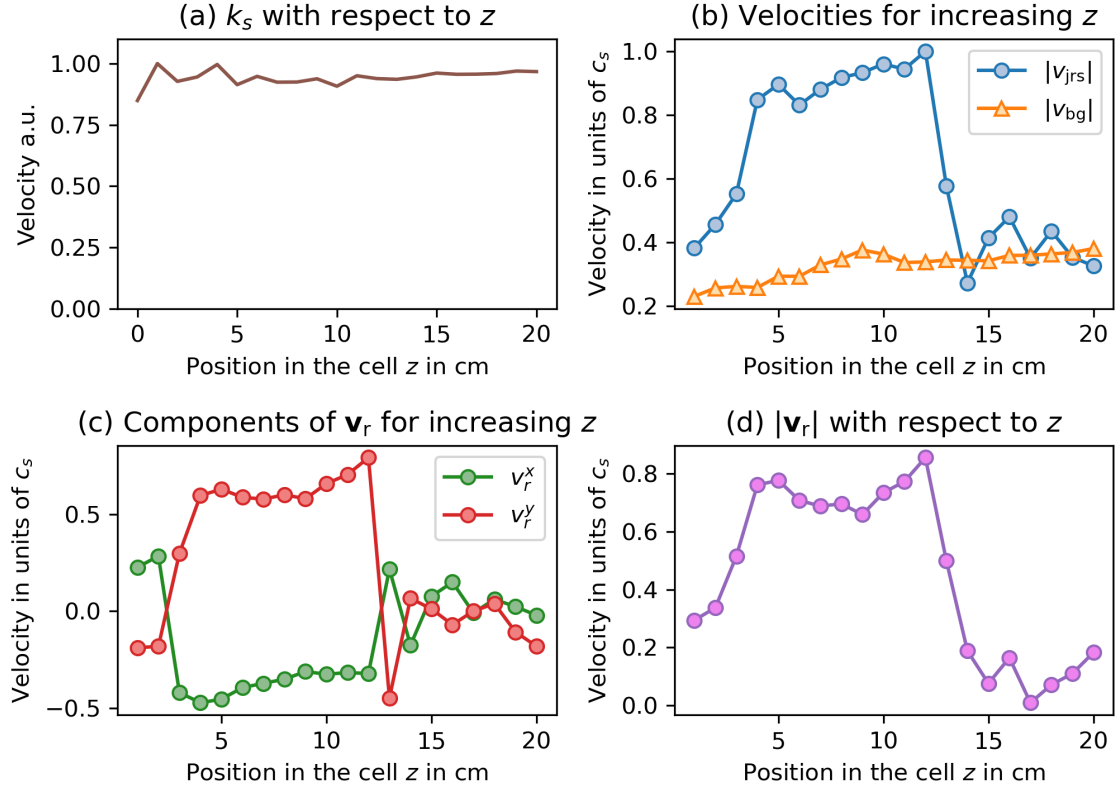


Figure 11: Results of the simulation of the SMV experiment. (a) Evolution of the speed of sound c_s with the position z inside the cell, (b) evolution of the JRS and background velocities for increasing z , (c) evolution of the components of \mathbf{v}_r for increasing z , (d) norm of \mathbf{v}_r with respect to z .

fig.11(a) and show a slowly varying value of c_s during propagation with deviations smaller than $\pm 10\%$. We can then average out the velocity field on a window of 10 px to obtain the evolution of \mathbf{v}_{jrs} and \mathbf{v}_{bg} with respect to z . We observe in fig.11(b) that there are **two distinct jumps** in the evolution of \mathbf{v}_{jrs} at $z = 3$ cm and $z = 12$ cm. By observing the phase of the field we discover that the first jump corresponds to the **fusion** of the two vortices used to generate the soliton while the second jump matches with the observation of a **breaking** of the soliton into a dipole.

As we did in section 3.3.2 we plot in panel (c) the components of the relative velocity \mathbf{v}_r computed using eq.21. We see that the merging and breaking of the dipole coincides with an inversion of the flow at its center, as observed in the experiment. We finally plot $|\mathbf{v}_r|$ in panel (d). This time, we measure a breaking relative velocity of approximately **0.8** c_s , slightly more than the experimental value. After the splitting, $|\mathbf{v}_r|$ goes to 0 as the vortices follow the background current.

This value is not to be taken as a general answer to the problem either because the flaws of the SMV experiment detailed in 3.3.2 also affect the simulation (namely the dependence on the window size, presence of non-trivial flows, and inhomogeneous density of the fluid). However, the similitude between the experimental and simulated results hints strongly

towards a theory where JRSs tend to break when their relative velocity **approaches the speed of sound**. To prove this theory and give precise values of the breaking velocity, more experiments and simulations need to be performed on trivial flows and homogeneous densities. On top of that, using the parameter \bar{v} from [33] in the measurement could allow us to get rid of the influence of the window size.

5 Conclusion

Paraxial fluids of light constitute a relatively new and expanding field of modern physics. Great progress made during the last decades demonstrates the potential of these systems to simulate fundamental properties of quantum matter. Observation and characterizing Jones-Roberts solitons opens up new possibilities to study the effects of modern hydrodynamical singularities which are difficult or impossible to observe in conventional cold atoms experiments. Results on the breaking dynamics of Jones-Roberts solitons obtained during my internship bring us one step closer to understanding effects such as superfluidity, non-equilibrium dynamics, and turbulence in quantum fluids.

Here we first developed a simplified theory of quantum fluids of light and their singularities. We then used off-axis interferometry to observe vortices and solitons in fluids of light and extract the critical breaking velocity. Finally, the dynamics of this breaking effect could be evaluated thoroughly through numerical simulation. Both approaches yielded velocities close to the sound velocity in the fluid hinting at a mechanism where breaking occurs when the speed of sound is locally exceeded. Additional experiments will be performed following the submission of this report. The experimental sequence will be simplified to simpler flows, density inhomogeneities will be taken into account and a new velocity parameter will be implemented to avoid pitfalls in the data processing. Results obtained during my internship will be shared via a poster presentation at the Wilhelm and Else Heraeus Foundation seminar on **Advances in Quantum Simulation and Sensing with Ultracold Gases** in Bad Honnef in June 2024.

In parallel to the work presented in this report, I also took part in the conception of a brand new cold atoms experiment as part of the **MistiQ-Light European project**. It will allow the generation, observation, and manipulation of fluids of light inside a cold atomic cloud of Rb atoms. My work on this project is to design and build the experimental apparatus as well as to find the optimal parameters for the study of fluids of light. This platform will hopefully allow us to tailor the potential in which the fluid of light evolves and thus observe a **quantum phase transition** from a superfluid state to a Mott insulator of photons.

References

- [1] Lev P. Pitaevskij and Sandro Stringari. *Bose-Einstein condensation and superfluidity*. Number 164 in International series of monographs on physics. Oxford University Press, Oxford, reprinted (with corrections) edition, 2016.
- [2] A. Amo, S. Pigeon, D. Sanvitto, V. G. Sala, R. Hivet, I. Carusotto, F. Pisanello, G. Leménager, R. Houdré, E. Giacobino, C. Ciuti, and A. Bramati. Polariton Superfluids Reveal Quantum Hydrodynamic Solitons. *Science*, 332(6034):1167–1170, June 2011.
- [3] J. Kasprzak, M. Richard, S. Kundermann, A. Baas, P. Jeambrun, J. M. J. Keeling, F. M. Marchetti, M. H. Szymańska, R. André, J. L. Staehli, V. Savona, P. B. Littlewood, B. Deveaud, and Le Si Dang. Bose-Einstein condensation of exciton polaritons. *Nature*, 443(7110):409–414, September 2006. Number: 7110 Publisher: Nature Publishing Group.
- [4] Frank Arute, Kunal Arya, Ryan Babbush, Dave Bacon, Joseph C. Bardin, Rami Barends, Rupak Biswas, Sergio Boixo, Fernando G. S. L. Brandao, David A. Buell, Brian Burkett, Yu Chen, Zijun Chen, Ben Chiaro, Roberto Collins, William Courtney, Andrew Dunsworth, Edward Farhi, Brooks Foxen, Austin Fowler, Craig Gidney, Marissa Giustina, Rob Graff, Keith Guerin, Steve Habegger, Matthew P. Harrigan, Michael J. Hartmann, Alan Ho, Markus Hoffmann, Trent Huang, Travis S. Humble, Sergei V. Isakov, Evan Jeffrey, Zhang Jiang, Dvir Kafri, Kostyantyn Kechedzhi, Julian Kelly, Paul V. Klimov, Sergey Knysh, Alexander Korotkov, Fedor Kostritsa, David Landhuis, Mike Lindmark, Erik Lucero, Dmitry Lyakh, Salvatore Mandrà, Jarrod R. McClean, Matthew McEwen, Anthony Megrant, Xiao Mi, Kristel Michielsen, Masoud Mohseni, Josh Mutus, Ofer Naaman, Matthew Neeley, Charles Neill, Murphy Yuezhen Niu, Eric Ostby, Andre Petukhov, John C. Platt, Chris Quintana, Eleanor G. Rieffel, Pedram Roushan, Nicholas C. Rubin, Daniel Sank, Kevin J. Satzinger, Vadim Smelyanskiy, Kevin J. Sung, Matthew D. Trevithick, Amit Vainsencher, Benjamin Villalonga, Theodore White, Z. Jamie Yao, Ping Yeh, Adam Zalcman, Hartmut Neven, and John M. Martinis. Quantum supremacy using a programmable superconducting processor. *Nature*, 574(7779):505–510, October 2019.
- [5] Quentin Glorieux, Tangui Aladjidi, Paul D. Lett, and Robin Kaiser. Hot atomic vapors for nonlinear and quantum optics. *New Journal of Physics*, 25(5):051201, May 2023. Publisher: IOP Publishing.
- [6] Pierre Azam, Adam Griffin, Sergey Nazarenko, and Robin Kaiser. Vortex creation, annihilation, and nonlinear dynamics in atomic vapors. *Physical Review A*, 105(4):043510, April 2022. Publisher: American Physical Society.
- [7] T. Bienaimé, M. Isoard, Q. Fontaine, A. Bramati, A. M. Kamchatnov, Q. Glorieux, and N. Pavloff. Quantitative Analysis of Shock Wave Dynamics in a Fluid of Light. *Physical Review Letters*, 126(18):183901, May 2021. arXiv:2101.00720 [cond-mat, physics:nlin, physics:physics].

REFERENCES

- [8] Myrann Abobaker, Wei Liu, Tangui Aladjidi, Alberto Bramati, and Quentin Glorieux. Inverse energy cascade in two-dimensional quantum turbulence in a fluid of light, November 2022. arXiv:2211.08441 [cond-mat, physics:quant-ph].
- [9] Jan Klaers, Julian Schmitt, Frank Vewinger, and Martin Weitz. Bose–Einstein condensation of photons in an optical microcavity. *Nature*, 468(7323):545–548, November 2010. Number: 7323 Publisher: Nature Publishing Group.
- [10] Florent Michel, Jean-François Coupechoux, and Renaud Parentani. Phonon spectrum and correlations in a transonic flow of an atomic Bose gas. *Physical Review D*, 94(8):084027, October 2016. Publisher: American Physical Society.
- [11] Claire Michel, Omar Boughdad, Mathias Albert, Pierre-Élie Larré, and Matthieu Bellec. Superfluid motion and drag-force cancellation in a fluid of light. *Nature Communications*, 9(1):2108, May 2018. tex.ids: michelSuperfluidMotionDragforce2018 tex.copyright: 2018 The Author(s) Number: 1 Publisher: Nature Publishing Group.
- [12] Tangui Aladjidi. *Full optical control of quantum fluids of light in hot atomic vapors*. phdthesis, Sorbonne Université, October 2023.
- [13] Robert W. Boyd. *Nonlinear Optics*. Elsevier, May 2008. Google-Books-ID: uoRUi1Yb7ooC.
- [14] Daniele Faccio, Paolo Di Trapani, Stefano Minardi, Alberto Bramati, Francesca Bragheri, Carlo Liberale, Vittorio Degiorgio, Audrius Dubietis, and Aidas Matijausius. Far-field spectral characterization of conical emission and filamentation in Kerr media. *Journal of the Optical Society of America B*, 22(4):862, April 2005.
- [15] Pierre-Élie Larré and Iacopo Carusotto. Propagation of a quantum fluid of light in a cavityless nonlinear optical medium: General theory and response to quantum quenches. *Physical Review A*, 92(4):043802, October 2015.
- [16] Iacopo Carusotto and Cristiano Ciuti. Quantum fluids of light. *Reviews of Modern Physics*, 85(1):299–366, February 2013. Publisher: American Physical Society.
- [17] Q. Fontaine, T. Bienaimé, S. Pigeon, E. Giacobino, A. Bramati, and Q. Glorieux. Observation of the Bogoliubov dispersion relation in a fluid of light. *Physical Review Letters*, 121(18), October 2018. tex.ids: fontaine2018Observation, fontaineObservationBogoliubovDispersion2018.
- [18] M. H. Anderson, J. R. Ensher, M. R. Matthews, C. E. Wieman, and E. A. Cornell. Observation of Bose-Einstein Condensation in a Dilute Atomic Vapor. *Science*, 269(5221):198–201, July 1995.
- [19] Immanuel Bloch, Jean Dalibard, and Sylvain Nascimbène. Quantum simulations with ultracold quantum gases. *Nature Physics*, 8(4):267–276, April 2012.
- [20] A. M. Kamchatnov and S. V. Korneev. Oblique solitons generated by the flow of a polariton condensate past an obstacle. *Journal of Experimental and Theoretical Physics*, 115(4):579–585, October 2012. tex.ids: kamchatnovObliqueSolitonsGenerated2012.

REFERENCES

- [21] S. Pigeon, I. Carusotto, and C. Ciuti. Hydrodynamic nucleation of vortices and solitons in a resonantly excited polariton superfluid. *Physical Review B*, 83(14):144513, April 2011. tex.ids: pigeon2011hydrodynamic tex.publisher: APS.
- [22] E. Madelung. Quantentheorie in hydrodynamischer Form. *Zeitschrift für Physik*, 40(3):322–326, March 1927.
- [23] Ashton S. Bradley and Brian P. Anderson. Energy Spectra of Vortex Distributions in Two-Dimensional Quantum Turbulence. *Physical Review X*, 2(4):041001, October 2012.
- [24] Marco Ornigotti, Shimshon Bar-Ad, Alexander Szameit, and Victor Fleurov. Analog gravity by an optical vortex: Resonance enhancement of Hawking radiation. *Physical Review A*, 97(1):013823, January 2018. Publisher: American Physical Society.
- [25] R. Navarro, R. Carretero-González, P. J. Torres, P. G. Kevrekidis, D. J. Frantzeskakis, M. W. Ray, E. Altıntaş, and D. S. Hall. Dynamics of a Few Corotating Vortices in Bose-Einstein Condensates. *Physical Review Letters*, 110(22):225301, May 2013.
- [26] D. J. Korteweg and G. De Vries. XLI. *On the change of form of long waves advancing in a rectangular canal, and on a new type of long stationary waves.* *The London, Edinburgh, and Dublin Philosophical Magazine and Journal of Science*, 39(240):422–443, May 1895.
- [27] Shunji Tsuchiya, Franco Dalfovo, and Lev Pitaevskii. Solitons in two-dimensional Bose-Einstein condensates. *Physical Review A*, 77(4):045601, April 2008.
- [28] K. Staliunas. Vortices and dark solitons in the two-dimensional nonlinear Schrödinger equation. *Chaos, Solitons & Fractals*, 4(8-9):1783–1796, August 1994.
- [29] A. M. Kosevich, V. V. Gann, A. I. Zhukov, and V. P. Voronov. Magnetic soliton motion in a nonuniform magnetic field. *Journal of Experimental and Theoretical Physics*, 87(2):401–407, August 1998.
- [30] Harry Proud, Marisa Perea-Ortiz, Charlotte O’Neale, M Baumert, M Holynski, Jochen Kronjäger, Giovanni Barontini, Kai Bongs, and Nadine Meyer. Jones-Roberts solitons defeating the snaking instability.
- [31] Y Kivshar. Dark optical solitons: physics and applications. *Physics Reports*, 298(2-3):81–197, May 1998.
- [32] Nadine Meyer, Harry Proud, Marisa Perea-Ortiz, Charlotte O’Neale, Mathis Baumert, Michael Holynski, Jochen Kronjäger, Giovanni Barontini, and Kai Bongs. Observation of Two-Dimensional Localized Jones-Roberts Solitons in Bose-Einstein Condensates. *Physical Review Letters*, 119(15):150403, October 2017.
- [33] L. A. Smirnov and V. A. Mironov. Dynamics of two-dimensional dark quasisolitons in a smoothly inhomogeneous Bose-Einstein condensate. *Physical Review A*, 85(5):053620, May 2012.

REFERENCES

- [34] F If, P Berg, P. L Christiansen, and O Skovgaard. Split-step spectral method for nonlinear Schrödinger equation with absorbing boundaries. *Journal of Computational Physics*, 72(2):501–503, October 1987.
- [35] Claude M. Dion and Eric Cancès. Spectral method for the time-dependent Gross-Pitaevskii equation with a harmonic trap. *Physical Review E*, 67(4):046706, April 2003.
- [36] R. Russell Rhinehart, Ming Su, and Upasana Manimegalai-Sridhar. Leapfrogging and synoptic Leapfrogging: A new optimization approach. *Computers & Chemical Engineering*, 40:67–81, May 2012.